Directed avalanche processes with underlying interface dynamics

Chun-Chung Chen and Marcel den Nijs

Department of Physics, University of Washington, Seattle, Washington 98195
(Received 18 February 2002; published 24 July 2002)

We describe a directed avalanche model; a slowly unloading sandbox driven by lowering a retaining wall. The directness of the dynamics allows us to interpret the stable sand surfaces as world sheets of fluctuating interfaces in one lower dimension. In our specific case, the interface growth dynamics belongs to the Kardar-Parisi-Zhang (KPZ) universality class. We formulate relations between the critical exponents of the various avalanche distributions and those of the roughness of the growing interface. The nonlinear nature of the underlying KPZ dynamics provides a nontrivial test of such generic exponent relations. The numerical values of the avalanche exponents are close to the conventional KPZ values, but differ sufficiently to warrant a detailed study of whether avalanche-correlated Monte Carlo sampling changes the scaling exponents of KPZ interfaces. We demonstrate that the exponents remain unchanged, but that the traces left on the surface by previous avalanches give rise to unusually strong finite-size corrections to scaling. This type of slow convergence seems intrinsic to avalanche dynamics.

I. INTRODUCTION

Avalanche phenomena are common in nature. Examples range from accumulating snow on mountain slopes, slow shearing between continental plates [1], rerouting in river networks, to creeping magnetic flux lines in super conductors [2]. Following the work by Bak *et al.* [3], physicists aim to capture the essential aspects of such dynamical systems with simple automaton processes, commonly referred to as sand-pile models and self-organized criticality (SOC). Impressive successes have been achieved, such as reproducing power-law distributions in avalanche events similar to those observed in nature, and the start of a classification scheme of such processes in terms of so-called universality classes [4]. Unfortunately most of these are numerical in nature. Analytical exact results remain rare.

Directed avalanche phenomena form a subclass of these SOC processes. Dhar and Ramaswamy introduced the first directed sandpile model and solved it exactly [5]. This was possible because in their model the avalanche propagation is governed solely by its two edges, and those two follow independent random walk dynamics. Tadić and Dhar introduced a directed model in which particles are allowed to pile up beyond the critical height, by replacing the automaton's deterministic toppling rule by a stochastic one [6]. The density of critical sites tunes itself and at distances far from the driving edge the propagation of active sites approaches the directed percolation [7] threshold. The scaling properties of the avalanche distributions are thus linked to the critical exponents characterizing the DP universality class. Another example of a stochastic directed avalanche process is the model introduced and studied numerically by Pastor-Satorras and Vespignani [8]. Similar as in the above model by Dhar and Ramaswamy, the stable landscape configurations (between avalanche events) lack internal correlations in the stationary state. This allowed Paczuski and Bassler [9] and also Kloster *et al.* [10] to link this dynamic process to so-called Edwards-Wilkinson [11] (EW) interface growth and to derive the exact scaling exponents of the avalanche distributions.

This novel world-sheet-type connection between avalanche dynamics and interface growth is particularly promising, because interface dynamic processes such as EW and Kardar-Parisi-Zhang [12] (KPZ) growth are very well understood, in particular, in $1+1$ dimensions ($1+1$D) where the scaling properties are known exactly. However, the above models that are linked to EW-type growth are rather poor examples, because EW growth is described by a simple linear stochastic (diffusion-type) Langevin equation; correlations factorize, and important caveats in the relation to avalanche dynamics can be obscured by this simplicity.

We set out to generalize this approach to nonlinear interface dynamic processes, and recently introduced a directed unloading sandbox model [13] in which the two-dimensional (2D) avalanche dynamics relates to $1+1$D KPZ-type interface growth. We derived exponent relations between the avalanche and interface growth scaling properties, which are generic, and valid beyond our specific model. Our numerical results for the avalanche distributions (for length, width, depth, and mass) follow indeed these exponent relations. Moreover, the avalanche critical exponents obey the predicted KPZ values within a few percent, an accuracy typical to avalanche simulations. However, our numerical accuracy is better than that; mostly because of a careful finite-size scaling (FSS) analysis. The exponents seem to converge to values that are slightly different from the KPZ values.

This left us with a puzzle. What is the origin of these small deviations? Is this a fundamental effect; or do the exponents ultimately converge to the KPZ values, but with unusually large corrections to scaling. In this paper we address these issues. We also provide a more detailed discussion of these world-sheet-type relationships between avalanche and interface growth dynamics. Our first paper was short and did not include many of the details that are crucial for the analysis presented here.

The fundamental difference between conventional KPZ interface growth and avalanche dynamics arises from the averaging process over KPZ-type space-time world sheets. In normal Monte Carlo (MC) simulations of interface growth

the distribution functions are determined in terms of ensemble averages over a set of totally uncorrelated space-time MC runs. In contrast, the avalanche dynamics gives rise to KPZ world sheets that are strongly correlated. Two subsequent MC runs are identical except inside a single avalanche area. This difference in averaging, uncorrelated versus avalanche-correlated MC runs, therefore emerges as a key issue for understanding the scaling properties of avalanche dynamics. This issue did not arise in the earlier EW-type avalanche models due to the linear nature of the EW process. However, for nonlinear dynamics, such as KPZ, avalanche-correlated-type sampling could well lead to novel interface scaling exponents.

Speaking against a shift in the values of the exponents, are arguments that: the KPZ stationary state, i.e., the sand surface profile far way from the driving edge, cannot be affected by the avalanche-correlated-type averaging, because large avalanches that span the entire width of the box occur periodically. These completely refresh the surface far away from the driving edge regularly, and thus wipe out all correlations between MC runs. This suggests that we are only dealing with much larger than usual corrections to scaling. The details are more complex than this simple argument, but we will establish that indeed the exponent values do not change.

The paper is organized as follows. In the following section, we present the unloading sandbox model. In Sec. III, we comment on how directed avalanche dynamics can be linked to interface growth in one lower dimension. Next, in Sec. IV, we show that in the interface growth interpretation our specific model belongs to the KPZ universality class. In Sec. V, we derive the generic exponent relations between interface growth and directed avalanche dynamics, and in Sec. VI we test this numerically for our specific model.

In the second half of this paper we address the small deviations in the numerical values of the exponents from those of conventional KPZ growth. In Sec. VII, we present numerical results detailing how the traces left on the surface profile by previous avalanches influence both the avalanche exponents and the interface growth ones. These scars in the rough surface enhance the surface roughness. We cast this enhanced interface roughness in terms of corrections to scaling, and determine what value the critical dimension of the corresponding irrelevant operator O_{sc} (in the sense of renormalization theory) should have. Next, in Sec. VIII, we identify the geometric meaning of O_{sc}, starting with a study of the one-dimensional version of our model where a similar phenomenon takes place. In 1D the interface growth process is a simple random walk, and the avalanche-correlated sampling relates to the scaling properties of merging random walkers. O_{sc} represents the distribution of avalanche end points in the 1D surface, and can be studied directly from the rounding of the surface profile near the driving edge. In Sec. IX, we return to the full 2D case. The scars of previous avalanches form lines on the surface. We identify O_{sc} with the angle these lines make with respect to the direction perpendicular to the driving edge, and confirm with an analytic argument that the critical dimension of O_{sc} is equal to x_{sc}
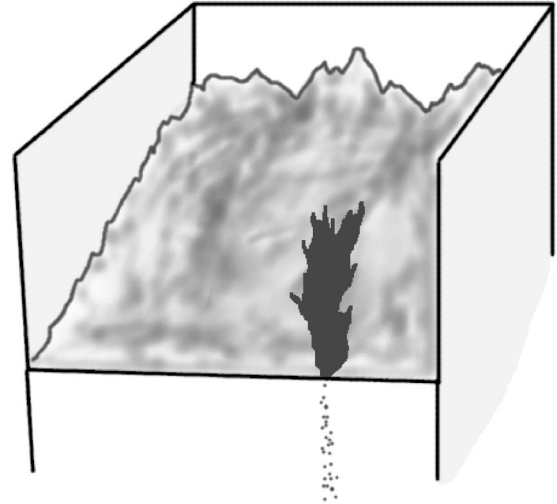

FIG. 1. Sandbox with a slowly lowering retaining wall.

$= -z$ with z the KPZ dynamic exponent. Finally, we summarize our results in Sec. X.

II. AN UNLOADING SANDBOX

Imagine a box filled with granular material, as illustrated in Fig. 1. One of its four retaining walls is slowly lowered, such that the sand spills out from that side, and thus slowly unloads the box and establishes a sloped surface. In the quasistatic limit, the wall moves slow enough that the unloading events can be described as distinct avalanches. The box can be three dimensional, leading to 2D avalanche dynamics on a 2D surface, or can be 2D (like in a very narrow box) giving rise to 1D avalanches on a 1D surface.

Inspired by this we consider a so-called solid-on-solid model defined on a 2D lattice. Height variables $h(\mathbf{r})$ are defined on a square lattice. We will consider two versions of the model. In the continuous height version, the heights are real numbers. In the discrete model, the heights are integers $h(\mathbf{r}) = 0, \pm 1, \pm 2, \ldots$. The former corresponds to a continuous material without internal structure, but strong cohesion up to a specific length scale s_c, while the latter corresponds to layered material where the surface height is quantized.

The 2D lattice is rotated diagonally such that the propagation direction of the avalanche is along the diagonal direction denoted by y. This is the direction in which the avalanche will run. Throughout this paper the coordinate perpendicular to y will be denoted by x. Figure 2 illustrates this geometry.

The configurations are subject to the following stability condition. The column of particles on site $\mathbf{r} = (x, y)$ is supported by the two columns $\mathbf{r}_l = (x-1, y-1)$ and $\mathbf{r}_r = (x+1, y-1)$ directly below it and is stable when its height is less than the minimum of the heights at these two supporting sites increased by a fixed amount:

$$h(\mathbf{r}) \leq \min[h(\mathbf{r}_l), h(\mathbf{r}_r)] + s_c , \tag{1}$$

where s_c is a constant. In the version of our model where the heights are continuous variables, s_c represents the only
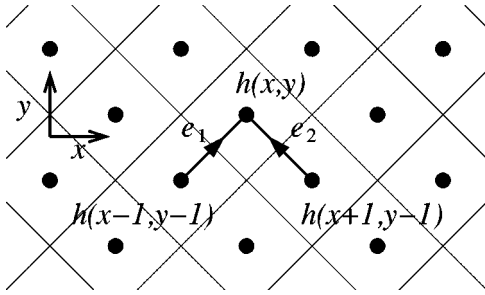
FIG. 2. Lattice structure of sandbox model in 2D.

length scale in the h direction and can be set equal to 1 without the loss of generality. Throughout this paper we will also set $s_c = 1$ in the discrete h model.

Consider a stable configuration, after $\tilde{t} - 1$ avalanches. The $\tilde{t}$th avalanche is triggered at the highest site $\mathbf{r} = (\mathbf{x}_{\tilde{t}}, 0)$, on the $y = 0$ driving boundary (or, in the discrete height model, by randomly choosing one of the highest sites) and reducing its height by a random amount $0 < \eta_{\tilde{t}} \leq s_c$. This likely creates unstable sites in the next $y = 1$ row. Those are updated by replacing their height by an amount equal to the lowest of the two supporting columns in the previous row and then adding an uncorrelated random amount $0 \leq \eta(\mathbf{r}) \leq s_c$ with uniform distribution, as

$$h(\mathbf{r}) \rightarrow \min[h(\mathbf{r}_l), h(\mathbf{r}_r)] + \eta(\mathbf{r}). \quad (2)$$

This updating continues row by row until all the sites are stable again. Only after that the next avalanche is started. The toppling of a site only affects the stability of the two sites immediately above it in the next y row. Therefore, we can update the system row by row in increasing order of y.

Direct experimental realizations of this unloading sandbox model are not our immediate concern (the focus is on establishing a generic theoretical relationship between avalanche dynamics and interface growth), but we expect that this model is applicable to actual experimental unloading sandboxes. One of the most important issues in this context is the row-by-row nature of the toppling rule. This is a crucial feature for our purposes, allowing the identification with KPZ interface growth (in the following section). In real unloading sandboxes the sand removed from row y rolls downhill and likely disturbs the already stabilized lower surface levels. Experimental realizations can avoid this from happening, e.g., by choosing very light grains (compared to the cohesion forces). Note that our dynamic rule does not allow the buildup of any pockets (deeper than s_c) on the surface that might trap such downward rolling grains.

Conservation laws are crucial to avalanche dynamics. Unlike most avalanche processes, our model does not conserve mass while the avalanche propagates. That might raise the specter of our model not being (self-organized) critical. The connection to KPZ growth (an intrinsic critical process) dispels this phantom. Moreover, the global slope of the surface is preserved during each avalanche run, and conservation of steps in the profile plays the role analogous to conservation of mass.

In a typical SOC process, the quasistatic limit must be taken such that the surface regains full stability before a new grain is being removed at the driving edge. Since avalanches of all sizes appear, this means that the velocity of the lowering wall should be inversely proportional to the size $L_x \times L_y$ of the box. Our process, however, is Markovian, i.e., row by row in the y direction. Removal of particles in row y does not affect the stability of the lower levels. In that case the lowering velocity needs only to be inversely proportional to L_x.

The analysis of the dynamics involves distribution functions of various characteristic features of the avalanches. The common examples are: length, width, depth, and mass. The avalanche length l will be defined throughout this paper as the maximum distance y the avalanche travels from the driving edge; the width w as the maximum departure of the x coordinate (perpendicular to the propagation direction) from the trigger point x coordinate; the depth δ as the maximum height change the avalanche creates at any of the affected sites; and the mass m as the total amount of material removed by the avalanche. All the above are dimensionless quantities measuring the numbers of lattice spacings (or multiples of s_c in the h direction) in our numerical presentations.

III. AVALANCHES VERSUS EPITAXIAL INTERFACE GROWTH

The focus of this paper is on how the above avalanche dynamics relates to interface growth in one lower dimension. Each stable sloped surface configuration of a directed sandpile can be reinterpreted as a world sheet (space-time configuration) of an interface in one lower spatial dimension. The direction in which the avalanches propagate plays the role of time and the perpendicular coordinates the role of space. Our 2D unloading sandbox is equivalent to a 1D growing interface. Such an interpretation makes sense only when the stability condition and the avalanche dynamic rule is directional and local in space time, such that causality is not violated in the interface growth interpretation. The stability condition (1) and toppling rule (2) of our model are row by row in nature and therefore indeed Markovian in this sense.

Every stable configuration of the sandpile represents a possible interface growth lifeline (space-time-evolution interface world sheet). The conventional procedure for determining the scaling properties of growing interfaces is to average over a large set of completely independent MC runs. This would mean, in sandbox language, an ensemble average over completely refreshed surfaces, each totally uncorrelated from the previous one (except typically for the initial condition in row $y = 0$). The toppling rule (2) is applied to all sites in every row, and repeated row by row, instead of only the unstable sites created by toppling only the highest site in the initial row.

In avalanche dynamics, however, two subsequent growing interface lifelines in this ensemble differ only inside the avalanche area. From the interface growth perspective this represents a rather peculiar and dangerous correlated-type MC run averaging procedure. The MC runs of KPZ space-time

configuration are strongly correlated, and this raises the specter of a change in the interface roughness scaling properties. The numerical evidence, presented below is sufficiently ambiguous that this issue will preoccupy us in the second half of this paper.

IV. KPZ GROWTH

In this section, we demonstrate that the interface growth model conjugate to the unloading 2D sandbox belongs to the 1+1D KPZ universality class. The time evolution of the interface is governed by the the toppling rule of the sand model with y in Eq. (2) representing time t,

$$h(x,t+1)=\min[h(x+1,t),h(x-1,t)]+\eta(x,t). \quad (3)$$

In the conventional global-type interface evolution (i.e., totally refreshing nonavalanche-type uncorrelated MC runs) every site in row $t+1$ is updated according to this rule.

Figure 3 illustrates the interface dynamics for one time step, $t \rightarrow t+1$. Conceptually, the time step can be split into two parts; the deterministic min[] operator part and the stochastic random deposition η part.

Note that because of the diagonal orientation of the square lattice (see Fig. 2), the lattice sites are not "stationary in time." The conceptually easiest interpretation to resolve this flip-flopping is to first double the number of lattice sites and then require them to be paired alternately with their right or left neighbors at even and odd times; at even times sites $2n$ and $2n+1$ are fused to be at equal heights and at odd times the $2n-1$ and $2n$ sites.

The upper panel shows the deterministic first half of the update (from the drawn to the dash line). The partners switch and the min[ ] operation equalizes their heights by choosing the lowest of the two, so this step always removes material.

This can be interpreted also in terms of a movement of the steps in the interface. All up steps move to the right and all down steps to the left; while up and down steps merge when they meet at one site.

The lower panel illustrates the second half of the update. The height of each fused pair increases by a random amount $0 \leq \eta \leq s_c$.

Deposition-type interface dynamics like this typically belongs to the KPZ universality class [12]. Indeed, Eq. (3) can be rewritten as

$$h(x,t+1)=\tfrac{1}{2}\left[h(x+1,t)+h(x-1,t)\right]$$
$$-\tfrac{1}{2}\left|h(x+1,t)+h(x-1,t)\right|+\eta(x,t), \quad (4)$$

and from this it can be easily identified to be a discrete form of the KPZ Langevin equation,

$$\frac{\partial h}{\partial t}=\nabla^2 h-\frac{\lambda}{2}(\boldsymbol{\nabla} h)^2+\eta. \quad (5)$$

The crucial point is that the coefficient of the nonlinear term λ is clearly present. There is no hidden special symmetry of some kind that makes it vanish by accident. At $\lambda=0$, the KPZ equation would reduce to EW growth.
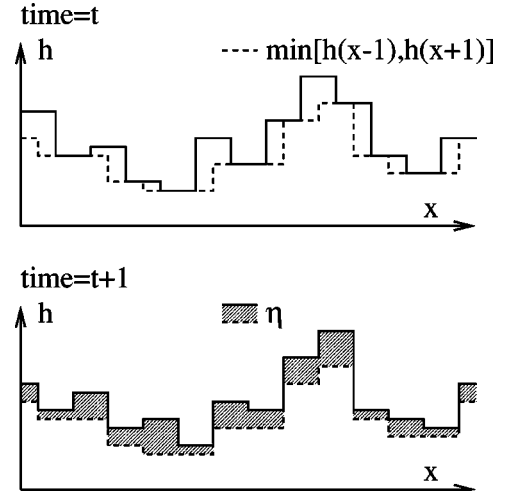

FIG. 3. The interface growth dynamics described by Eq. (3) with upper panel showing movement of steps (from the drawn to dashed line) and lower panel random depositions (shaded area) to the interface.

To confirm the KPZ nature and make sure that the λ is large enough that corrections to scaling from the EW point ($\lambda=0$) are not obscuring the KPZ scaling, we perform MC simulations on the interface dynamics as illustrated in Fig. 3. The MC runs are completely independent.

We measure the time evolution of the interface width W defined as

$$W^2(L_x,t)\equiv\overline{\langle(h-\bar{h})^2\rangle} \quad (6)$$

with over bars (angle brackets) indicating average over x (ensemble). Starting from, e.g., a flat initial condition it should scale as

$$W \sim t^\beta \quad (7)$$

at intermediate times $0 \ll t \ll L_x^z$, and saturate at

$$W \sim L_x^\alpha \quad (8)$$

for $t \gg L_x^z$; with L_x the length of the 1D interface. The exponents for the KPZ universality class in 1+1D are known exactly with $\alpha=1/2$, $\beta=1/3$, and $z \equiv \alpha/\beta=3/2$.

The numerical results are shown in Fig. 4. The values of $\alpha(L_x)$ are obtained from the saturated interface widths by imposing the scaling form (8) at adjacent values of the system size L_x. Similarly, the values of $\beta(t)$ are obtained from the transient interface widths by imposing the scaling form (7) at nearby times t. We like to remind the reader that simple log-log plots of W versus L_x and t look typically impressively straight, but are notoriously inaccurate. The construction of effective exponents, in the above manner might at first glance look less impressive (the data appears noisier), but this brings the analysis to a higher level where the leading corrections to finite-size and finite-time scaling become visible.

The approach to $L_x \rightarrow \infty$ in Fig. 4 is consistent with the leading correction to scaling exponent $y_{ir} = -1/2$ expected from the EW term $\nabla^2 h$ in Eq. (5). The corrections to FSS are stronger when the height variables are discrete than when they are continuous. This is consistent with the smaller growth rate in the discrete height interface, and the fact that the growth rate is typically proportional to the nonlinear term λ. On average, more material is removed during the first deterministic part of the update process when the surface heights are discrete.

V. SCALING PROPERTIES OF 2D AVALANCHES

In this section, we derive the exact relations between the scaling properties of the avalanches and $1+1D$ KPZ interface growth. However, in the latter the world sheets are sampled in the correlated manner as outlined in Sec. III.

The characteristic feature of SOC is the lack of typical avalanche length, width, depth or mass scales. The probability distributions follow power laws. For example, the distribution of avalanche widths scales as

$$P_w \sim w^{-\tau_w} \qquad (9)$$

with scaling exponent τ_w. Similarly, the avalanche length, depth, and mass distributions scale as power laws with exponents τ_l, τ_δ, and τ_m. We can summarize this in a meta-distribution function $P(l,w,\delta)$; the probability to find an avalanche of a specific width w, length l, and depth δ obeys the scaling relation

$$P(l,w,\delta) = b^{-\sigma} P(b^{-z}l, b^{-1}w, b^{-\alpha}\delta) \qquad (10)$$

with b an arbitrary scale parameter. The exponents σ, z, and α are expected to be robust with respect to details of the dynamic rule, and thus are characteristic of the universality class to which this avalanche dynamics belongs. Single parameter distributions, such as P_w, follow by integrating out the other variables. This implies the following expressions for the τ exponents:

$$\tau_l = \frac{\sigma - 1 - \alpha}{z}, \quad \tau_w = \sigma - z - \alpha, \quad \tau_\delta = \frac{\sigma - 1 - z}{\alpha}, \quad (11)$$

or inverted

$$z = \frac{\tau_w - 1}{\tau_l - 1}, \quad \alpha = \frac{\tau_w - 1}{\tau_\delta - 1}, \quad \sigma = \tau_w + z + \alpha. \qquad (12)$$

Let us presume that the avalanches are compact, i.e., that the inside and the boundaries of an avalanche are well defined and distinguishable (unlike in certain fractal structures), and that the sizes of the holes (unaffected regions) inside the avalanche do not scale with the avalanche size. This can be checked visually from typical simulation configurations, and both assumptions are indeed satisfied in our dynamics at least qualitatively. In that case, the mass of the avalanche must scale as $m \sim l w \delta$, such that the critical exponent of the distribution of avalanche masses $P_m \sim m^{-\tau_m}$ obeys the identity
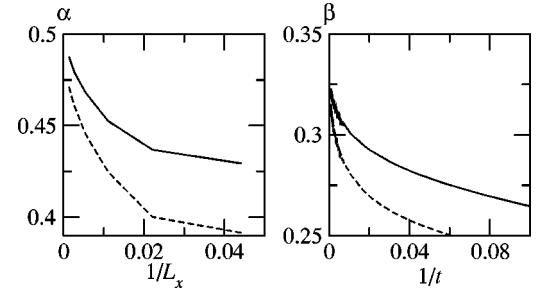

FIG. 4. MC results for the global interface width: left, finite-size (L_x, in the unit of lattice spacing) estimates for the saturated surface width exponent α; right, finite-time (t, in MC time steps) estimates for the transient interface width exponent β from a flat initial configuration. The solid (dashed) curves are for continuous (discrete) height model.

$$\tau_m = \frac{\sigma}{1 + z + \alpha}. \qquad (13)$$

There is one more relation between these critical exponents (leaving only two independent ones). The avalanche is initiated by lowering the bar at the driving edge of the box. In the stationary state the average surface profile is invariant, and therefore it shifts down at the same rate as the lowering bar. Thus, we know how much mass drops out of the box on an average.

To be more precise, during each avalanche event, the height of only one single boundary site at $y = 0$ is lowered by, on average, an amount $s_c/2$. For a sandbox of width L_x the boundary row is lowered by $s_c/2$ after L_x avalanches. In the stationary state, the entire surface matches this lowering speed, such that the amount of removed sand is on an average equal to $L_x L_y s_c/2$. Therefore, the average mass of each avalanche must be equal to

$$\langle m \rangle = \tfrac{1}{2} s_c L_y. \qquad (14)$$

The scaling properties of the mass distribution function tie into this because

$$\langle m \rangle = \int m' P_m(m') dm', \qquad (15)$$

which can be evaluated using the metadistribution function as

$$\langle m \rangle \sim \int_0^{L_y} dl \int_0^\infty dw \int_0^\infty d\delta\, lw\delta P(l,w,\delta)$$

$$+ m_{L_y} \int_{L_y}^\infty dl \int_0^\infty dw \int_0^\infty d\delta\, P(l,w,\delta). \qquad (16)$$

This equation incorporates finite-size effects. The box is presumed to be wide and deep enough, such that the length L_y of the box (in the direction perpendicular to the driving edge) is the only limiting finite-size factor. The first term in the above equation accounts for all avalanches that fit inside the box and the second term for the ones that reach the L_y edge, and thus are prematurely terminated. The first integral
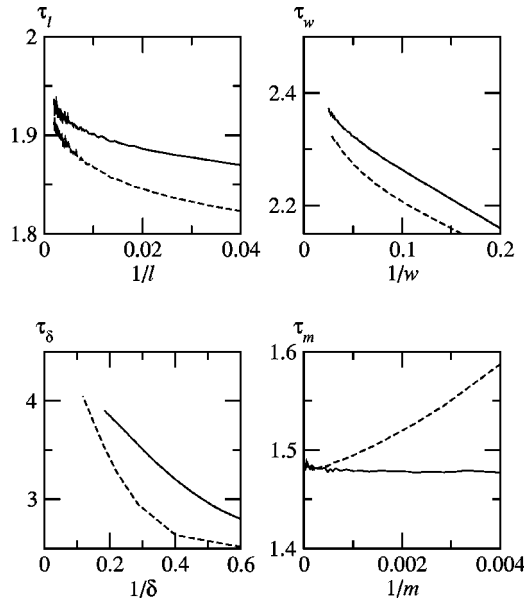
FIG. 5. FSS plots for the τ exponents of 2D sandbox model. The solid (dashed) lines are for continuous (discrete) height model.
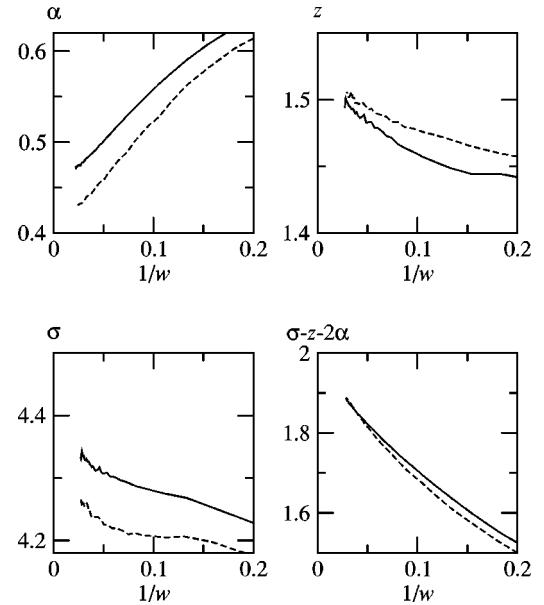

FIG. 6. Effective scaling exponents derived from stationary avalanche distributions of sandbox systems. The solid (dashed) lines are for continuous (discrete) height model.

scales as $L_y^{(-\sigma+2+2z+2\alpha)/z}$ for large L_y. The second term scales with the same power because the second integral scales as $L_y^{(-\sigma+1+z+\alpha)/z}$, while the mass factor in front of it scales as $m \sim l w \delta \sim L_y^{(1+z+\alpha)/z}$. The result

$$\langle m \rangle \sim L_y^{(-\sigma+2+2z+2\alpha)/z}, \tag{17}$$

when compared to Eq. (14), yields the exponent identity

$$\sigma = 2 + z + 2\alpha. \tag{18}$$

The validity of these exponent identities goes well beyond our KPZ-type unloading sandbox. For example, the EW-type directed avalanche models by Paczuski and Bassler [9] and Kloster et al. [10] obey our Eq. (11) when we substitute for z and α the EW values ($z=2$, $\alpha=1/2$). The scaling exponents of the original Dhar-Ramaswamy model can be described by the same equations with $z=2$, $\alpha=0$ as well.

VI. NUMERICAL RESULTS FOR 2D SANDBOX AVALANCHES

The discussion of the preceding section leaves us with two independent avalanche critical exponents, α and z. The notation anticipates their identification with the scaling properties of a rough interface in interface growth. There, α is the scaling exponent of the interface width and z the dynamic critical exponent. Indeed, the interface width relates to the depth of the avalanche, and time to the length of the avalanche. We expect therefore that α and z take same values as in 1+1D KPZ growth, $\alpha+z=2$ and $\alpha=1/2$.

We perform MC simulations on the sandbox avalanche model and measure the avalanche metadistribution function $P(l,w,\delta|L_y)$ [see Eq. (10)]. The sandbox is always taken wide and deep enough such that the box length L_y acts as the only FSS-type limiting factor. We average over 2^{31} ava-

lanches. The reduced distributions, such as $P_l \sim l^{-\tau_l}$, follow from the metadistribution from, e.g., summation over w and δ.

Figure 5 shows FSS approximates for the τ exponents. They are constructed as follows. Power-law-decaying objects such as $P_l \sim l^{-\tau_l}$ are almost always subject to crossover-scaling-type effects, i.e., subdominant additional power-law terms. In the language of renormalization theory they originate from so-called irrelevant scaling fields and also from nonlinear scaling field effects. This is well documented in equilibrium critical phenomena, but most recent nonequilibrium scaling studies ignore this systematic effect, e.g., by simply making a log-log plot of P_l as function of l and drawing a least-square-fitting-type straight line through the data. Such results show very little statistical noise, but can give rise to significant systematic errors. An example of the importance of corrections to scaling, was the large spread in reported values of the stationary state roughness exponent α between various 2D KPZ-type-growth lattice models, which was resolved using a similar FSS analysis as presented here [14].

In the limit of large l the subdominant additional power-law terms fade away. So, more weight must be put on the large l part of the data than on the short l section. However, it is a balancing act, because at large l the results become noisier, since few avalanches reach that far.

The total number of avalanches that reach beyond y scales as

$$Q_l(y) = \int_y^\infty P_l(l) dl \simeq \frac{A}{\tau_l} y^{-\tau_l + 1}, \tag{19}$$

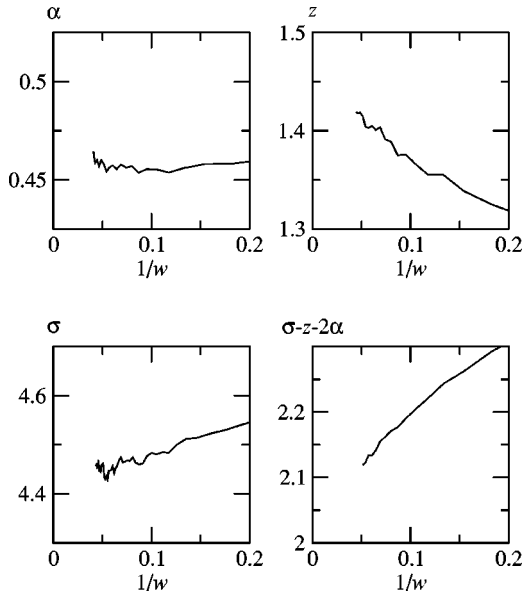if the fraction of avalanches of length y scales as P_l

FIG. 7. Effective scaling exponents derived from the distributions of first avalanches on fresh sandbox surface for the continuous height model.
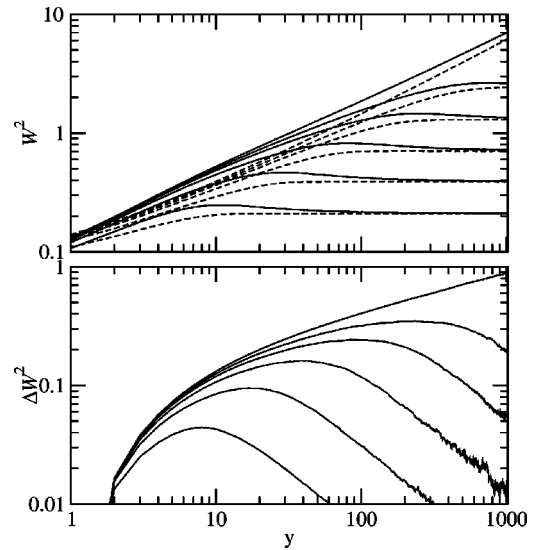

FIG. 8. Upper panel: The interface width (squared) for sandbox surface (solid lines) and the same for an ensemble of fresh surface (dashed lines); Lower panel: The difference between the two, with $L_x = 8$, 16, 32, 64, 128, and ∞ (from bottom up) the box size in the direction parallel to the driving edge.

$\simeq Ay^{-\tau_l}$ (these are only the leading terms). We construct a y dependent approximate for the exponent τ_l from the ratio of these two quantities, as

$$\tau_l(y) = \frac{lP_l(y)}{Q_l(y)}. \qquad (20)$$

The results are shown in Fig. 5. (We do the same for the other distributions.) Plots such as this are intrinsically noisier than conventional simple log-log type of plots of the distributions, but they contain much more information. The variation with y reflects the leading corrections to scaling. The statistical noise at large y could be suppressed by running the MC simulation longer. The simulation time is the only limiting factor. We used 2^{31} avalanches and in that case, $L_y = 512$ is the optimal box size.

In Fig. 6, we replot the same data in terms of α, z, and σ, following Eq. (12) and using the same type of FSS analysis. From the trend of the curves, we conclude that $\alpha = 0.46 \pm 0.01$, $z = 1.52 \pm 0.02$, $\sigma = 4.43 \pm 0.05$, and $\tau_m = 1.48 \pm 0.01$. This means that the exponent relations (13) and (18) are satisfied well within the statistical noise limitations, i.e., within a few percent.

Surprisingly, the actual values for z and α, although close, differ significantly from the exactly known $1+1$D KPZ values $\alpha = 1/2$ and $z = 3/2$. They deviate more than warranted from statistical noise alone, and do not converge smoothly if the KPZ values are correct. The approximates for α actually undershoot the KPZ value $\alpha = 1/2$, and those for z overshoot $z = 3/2$. This systematic effect needs to be explained. It could be that the exponents differ in a fundamental manner from the conventional KPZ values, or that we are looking at unusually large and slow corrections to FSS. The smallness of the deviations makes the latter more likely (except when this happens to be a continuously varying exponents scenario).

We will blame the correlated MC averaging feature for this, but it should be noted that avalanche distributions are intrinsically more sensitive to FSS effects than global interface features. Many avalanches in the ensemble are small compared to the global box size, and therefore sample and average the KPZ scaling properties over much smaller lengths and shorter time scales than in a conventional global interface roughness analysis at a comparable space-time box size.

One option is to push the run button on the computer and out perform all corrections to FSS. Unfortunately, it would require extremely long MC times to create large numbers of such large avalanches. It is doubtful that we would be able to get far enough in a reasonable time span. Moreover this approach is intellectually unappealing. We prefer to search for the origin of the deviations in the exponents.

VII. AVALANCHE-CORRELATED MC RUNS

The basic premise of our exponent identities is that avalanches are like any other fluctuation on a $1+1$D KPZ-type world sheet. Initially flat KPZ interfaces (the sand surface next to the driving edge) roughen in time (moving away from the driving edge) in such a manner that at (KPZ) time y the stationary state roughness is established within a length scale $l_x \sim y^{1/z}$. This defines a so-called spreading cone. The avalanches are expected to follow the same pattern. However, the avalanche cone seems to spread slightly faster, since the above avalanche value for z slightly exceeds the conventional KPZ value, and inside the avalanche the surface seems to be slightly less rough, since the avalanche value for α is slightly smaller.

In this and the following section we will establish that this is caused by correlations with previous avalanches. The new avalanche does not run its course on a pristine fresh KPZ
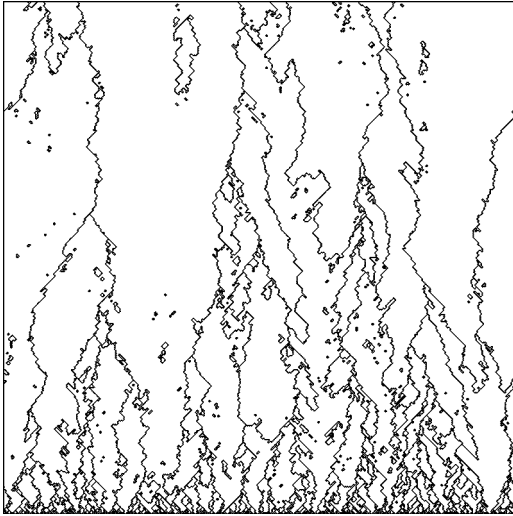
FIG. 9. A typical configuration of the scars on the sandbox created by the avalanches. The driving edge is located at the bottom of the graph while avalanches propagate upward in the y (or t) direction. The system sizes are $L_x = 256$ and $L_y = 512$.

interface world sheet but on an aged one scarred by previous avalanches.

There are two obvious tests to address the effects of these scars. The first one is to determine the avalanche distributions for only the first avalanche on a fresh KPZ world sheet (the initial condition), i.e., to refresh the entire surface completely after each avalanche. The results are shown in Fig. 7. The first avalanches likely follow normal KPZ exponents: z converges now smoothly towards $z = 3/2$; while the FSS approximates for α, although still too small, start to turn towards $\alpha = 1/2$ and do not cross that value anymore. It should be noted that the FSS corrections are expected to be larger, and that the data is noisier than in Fig. 6, because although we ran the same number of avalanches (2^{31}), the fraction of large avalanches is smaller, leading to smaller and noisier amplitudes in the power-law tails of the distributions.

The second test of the role of the scars is to measure the global interface roughness for avalanche-type correlated MC runs instead of completely refreshing MC runs. The upper panel of Fig. 8 shows the global interface width W^2 as function of time for several L_x's. The drawn lines correspond to avalanche-correlated MC runs and the dashed line to conventional uncorrelated MC averaging. The drawn lines have bumps, i.e., the avalanche-correlated runs lead to rougher interfaces at intermediate times.

This enhanced interface roughness is caused by the scars left by earlier avalanches. The scars vanish at very large y because avalanches reaching that far span the entire system in the x direction. Figure 9 shows a typical configuration of scars. The lines are the traces of previous avalanches, i.e., their edges. Latter avalanches wipe them out partially.

For finite system sizes, the stationary state interface width follows from the plateaus at large times. There the avalanche-correlated and uncorrelated MC curves coincide. This is to be expected, because the large avalanches that span the entire system (in the x direction at large y) occur at regular MC time intervals, such that the large y part of the surface (i.e., the stationary state of the growth process) is completely refreshed periodically and therefore sampled effectively like in uncorrelated MC runs. As a result, the roughness exponent α, defined by Eq. (8), is the same for the both cases.

Most avalanches do not extend into that large y part of the surface. They terminate in the scarred part of the surface. Therefore, we define an alternative roughness exponent α^*, associated with the scaling of the bumps, in terms of the maximized width

$$W^* \equiv \max_y W(L_x, y) \sim L_x^{\alpha^*} \qquad (21)$$

more relevant for the avalanche scaling properties. Note that for uncorrelated MC runs, $\alpha^* = \alpha$, since the interface width increases monotonically in time.

The conventional method for measuring the exponent β, involves the slope at times $y < L_x^z$, and thus is sensitive to the bumps in W as well. The results are shown in Fig. 10. Compared to those in Fig. 4, they clearly converge less smoothly, with larger corrections to scaling and we should wonder if they converge to the conventional exact KPZ values $\alpha = 1/2$ and $\beta = 1/3$, at all.

In the lower panel of Fig. 8 we plot ΔW^2 as function of time, the difference between the squared widths of avalanched-correlated MC runs (the drawn lines in the upper panel) and completely uncorrelated MC runs (the dashed lines in the upper panel). For infinite system size, ΔW^2 scales as $\Delta W^2 \sim y^s$ with an exponent that numerically is very close to $s \simeq 1/3$. Since the width itself scales as $W^2 \sim y^{2/3}$, it follows that the bumps in the width curves are a transient FSS effect.

This settles our basic issue at the numerical level; the avalanche-correlated nature of the MC runs does not change the interface scaling exponents, but only gives rise to slow corrections to FSS. In the following two sections, we will identify these corrections to scaling with the scars on the surface left behind by previous avalanches.

We start this analysis here by casting the deviations into the framework of corrections to scaling from a so-called irrelevant operator in the sense of renormalization theory. Let $O_{sc}(x)$ be the irrelevant operator and u be its scaling field.
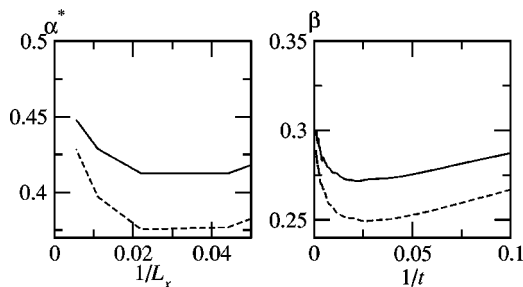

FIG. 10. Finite-size approximates of the scaling exponents for stationary surface of sandbox (or correlated MC runs for the interface model) with α^* defined by Eq. (21) and β by Eq. (7). The solid (dashed) curves are for the continuous (discrete) height model.

This amounts to presuming that the avalanche correlation between MC runs can be represented effectively by adding to the KPZ Langevin equation (5), a term $uO_{sc}(x)$. We will have to determine below how $O_{sc}(x)$ is related to the density of scars on the interface space-time world sheet left by previous avalanches. According to scaling theory, the presence of such a term to the Langevin equation leads to corrections to scaling in the interface width as

$$W^2(L_x, y, u) = b^{2\alpha} W^2(b^{-1}L_x, b^{-z}y, b^{y_{sc}}u), \quad (22)$$

i.e., in the infinite-size limit, $L_x \to \infty$, to

$$W^2(y, u) = y^{2\alpha/z} S(y^{y_{sc}/z}u), \quad (23)$$

and by expanding the scaling function S, while assuming that $y_{sc} < 0$, such that $u = 0$ is a stable fixed point, and the argument $y^{y_{sc}/z}u$ is a small parameter, to

$$W^2(y, u) = y^{2\alpha/z}[S(0) + y^{y_{sc}/z}uS'(0) + \cdots]. \quad (24)$$

The critical exponent y_{sc} of this irrelevant scaling field must take the value $y_{sc} = -\alpha$ to account for the $\delta W^2 \sim y^{1/3}$ corrections in the interface width we found above. Moreover, the operator must scale as

$$O_{sc}(x) \sim b^{-x_{sc}} \quad (25)$$

with critical dimension $x_{sc} = z$, since the KPZ equation (5), implies that the terms $uO_{sc}(x)$ and $\partial h/\partial t$ must scale alike. In the following two sections, we will trace down the geometric identity of this mysterious operator O_{sc}, starting with the 1D version of the model.

VIII. SURFACE ROUNDING IN THE 1D UNLOADING SANDBOX

The 1D version of the unloading sandbox shows the same type of differences between uncorrelated and avalanche-type-correlated MC runs as the 2D version. We determined numerically the difference between the interface width for avalanche-correlated and uncorrelated MC runs, and found that it diverges as a power law $\delta W^2 \sim y^{1/2}$, with an exponent that is again (like in 2D) half the size of that for $W^2 \sim y$ itself. According to the corrections to scaling formalism (24), the scaling dimension of O_{sc} must therefore be equal to $x_{sc} = z$, just as in 2D.

The underlying interface dynamics becomes a zero-dimensional growth model, i.e., a simple random walk in the h direction with a nonzero drift velocity to account for the net tilt of the surface. The exponents of the various avalanche distribution functions must obey the same type of relations as in Sec. V:

$$\tau_l = \frac{\sigma - \alpha}{z}, \quad \tau_\delta = \frac{\sigma - z}{\alpha}, \quad \tau_m = \frac{\sigma}{\alpha + z}, \quad (26)$$
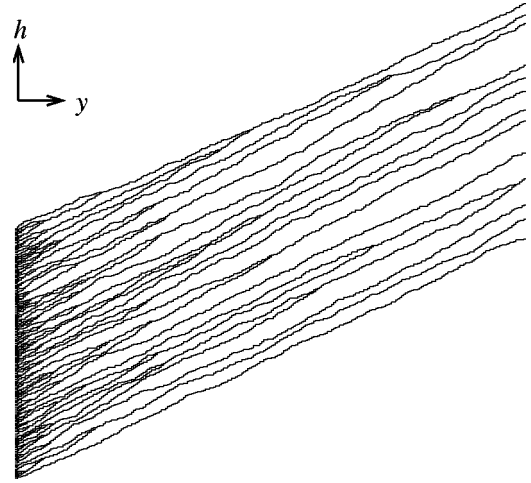
and

$$\sigma = z + 2\alpha. \quad (27)$$

FIG. 11. Traces of stable sand surface over 256 avalanches for 1D sandbox model with $L_y = 256$. The system is driven from the left at $y = 0$.

Without loss of generality we can set $\alpha = 1$ (measure all lengths in terms of δ). These identities are satisfied exactly, and the exponents are the same for uncorrelated and avalanche-correlated runs. From the interface dynamics perspective, a single directed random walker, the diffusion equation character of the dynamics implies that $z = 2\alpha = 2$. The values of all the other exponents follow from this, and are consistent with their values from the avalanche perspective. There, we are dealing with the statistics of merging random walkers. The number of walkers at a given "time" y is equal to the number of avalanches of a length l equal or larger than y in the ensemble of MC runs. The density of the walkers decays as $\rho(y) \sim y^{-1/2}$ [15], such that the distribution of avalanche lengths obeys the form

$$P_l(l) = \left[-\frac{\partial}{\partial y}\rho(y)\right]_{y=l} \sim l^{-3/2}, \quad (28)$$

and therefore that $\tau_l = 3/2$. The depth of the avalanche follows from the maximum separation between two subsequent walkers, and scales as $\delta \sim l^{1/2}$, i.e., $\alpha/z = 1/2$. The mass scales as $m \sim l\delta \sim l^{3/2}$, i.e., $(\alpha + z)/z = 3/2$ and $\tau_m = 4/3$.

This can be compared directly with the exponents of other 1D sandpile models, e.g., with results by Paczuski and Boettcher [16] on the so-called Oslo sandpile model, where $\tau \equiv \tau_m \approx 1.55$ and $D \equiv (\alpha + z)/z \approx 2.23$.

Let us turn our attention now to the central issue, the difference between uncorrelated versus avalanche-correlated MC runs. Adding a term such as uO_{sc} to the diffusion equation of motion creates a correction to the drift velocity of the random walk. This suggests that we can identify the geometric meaning of O_{sc} directly by studying the deviations of the slope near the driving edge of the surface from its asymptotic value.

The average surface slope does not show any deviations (near the driving edge) from $s_c/2$ when we run the dynamics as a conventional random walk, which amounts to "completely refreshing" the surface after each MC run (uncorre-

lated MC runs). The avalanche-correlated runs do show a rounding of the surface near the driving edge,

$$s(y) \simeq A y^{-\kappa} + \frac{1}{2} s_c . \qquad (29)$$

The numerical results for the exponent yield $\kappa = 0.98 \pm 0.03$. This confirms our corrections to scaling picture, because it predicts that $x_{sc} = z$ from the interface width since $\kappa = x_{sc}/z$ and $z = 2$ for random walks.

This rounding originates from the distribution of termination points of the avalanches. A new random walk starts below the previous one and propagates until it meets the previous trajectory and terminates. The avalanche is the space between the trajectory of that new random walk and the already existent surface. The amount of rounding of the slope near the driving edge is proportional to the distribution $\rho(y)$ of merging points on the surface. These merging points represent the scars left from previous avalanches. Each random walker by itself does not contribute to the rounding, i.e., on average each has a constant slope $s_c/2$. However, every new walk lies below the previous surface, such that down stream from every avalanche end point the surface is systematically lower than beyond it. This upward bias across the avalanche merging points (by an amount, e.g., $s_c/2$, on an average, in the discrete h version of our model) gives rise to the surface rounding and yields that the latter is proportional to $\rho(y)$.

The entire process and the set of subsequent stable sand surfaces (Fig. 11) is therefore equivalent to a system of merging random walkers obeying the rule $A + A \rightarrow A$. That type of dynamics has received extensive attention recently and its various scaling properties are known exactly [15]. There is little doubt that our 1D unloading sandbox is exactly soluble, using absorbing-wall-type random walk mathematics [17]. However, we will refrain from pursuing this path in this paper.

The critical dimension of $O_{sc} \sim \rho(y)$ can be estimated (for intuition building purposes) as follows. After adding a term $u O_{sc}$ to the KPZ equation we should also write down an equation of motion for O_{sc} itself, to close the equations. The latter is not trivial, because the scars on the surface build up slowly in time, such that that the equation of motion for O_{sc} is highly nonlocal. On the other hand, the linear nature of the diffusion equation allows one to be somewhat frivolous with the order in which averages are taken (without losing the essential physics, nor even the correct critical exponents).

Let $\rho_{\tilde{t}}(y)$ be the end-point distribution after $\tilde{t}$ avalanches (MC time steps). During the last MC time step, one avalanche runs through the system. It refreshes the entire surface before its termination point $y = l_{\tilde{t}}$, such that $\rho_{\tilde{t}}$ at site y does not change if the avalanche terminates before y; $\rho_{\tilde{t}}(y) = 1$ if it terminates at y; and $\rho_{\tilde{t}}(y) = 0$ if it extends beyond y:

$$\frac{\partial \rho_{\tilde{t}}(y)}{\partial \tilde{t}} = P_l(y) - \rho_{\tilde{t}}(y) \int_y^{\infty} P_l(l) dl \qquad (30)$$

with $P_l(l)$ the probability that the avalanche terminates at distance l from the driving edge. The stationary state endpoint profile therefore takes the form
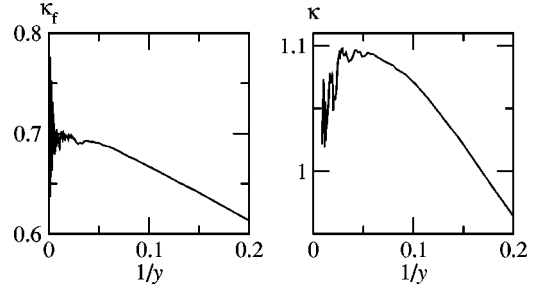

FIG. 12. Scaling exponent for boundary correction to the local slope of fresh 2D sandbox surface (or, in the interface language, transient growth rate from a flat interface), $s_f(y) - s_f(\infty) \sim y^{-\kappa_f}$, and its correction due to the iterated avalanche process, $\Delta s = s(y) - s_f(y) \sim y^{-\kappa}$.

$$\rho(y) = \frac{P_l(y)}{\int_y^{\infty} P_l(l) dl} , \qquad (31)$$

and $P_l(l) \sim l^{-\tau_l}$ yields

$$\rho(y) = \frac{1}{\tau_l - 1} y^{-1} . \qquad (32)$$

In other words, the surface curvature scales as $\Delta s \sim y^{-x_{sc}/z}$ with $x_{sc} = z$, in agreement with the above results. Interestingly, this result is independent of the actual value of the scaling exponent τ_l provided that $\tau_l > 1$, which has to be true for P_l to be normalizable.

In conclusion, in 1D we identified the crossover scaling operator with the density of avalanche end points. These represent indeed the scars on the surface, the memory of previous avalanches.

IX. AVALANCHE ROUNDING NEAR THE DRIVING EDGE IN 2D

As in the 1D model, the surface slope is modified by the iterated avalanche process. However, unlike in 1D, the average slope near the edge is not constant already in conventional interface dynamics (where the entire surface is being refreshed during each MC run). The surface slope is related to the growth rate of the underlying interface, and the rounding of the slope near the driving edge represents the transient
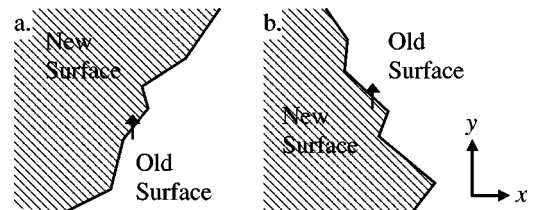

FIG. 13. Two possible cases at a boundary of an avalanche cluster (the shaded area): (a) avalanche expands; (b) avalanche shrinks. The local slopes along the arrow marks is reduced in (a) while increased in (b).

growth rate of the KPZ interface from the initial configuration, e.g., a flat one:

$$s_f(y) \simeq v_0 + c y^{-\kappa_f} \qquad (33)$$

with y playing the role of time and the subscript f denoting that the entire surface is refreshed. By direct numerical simulation of uncorrelated interface dynamics, we find $\kappa_f \approx 0.7$ (the left panel of Fig. 12). This is consistent with conventional KPZ scaling and power counting

$$s \sim h/y \sim y^{\alpha/z-1} \sim y^{-2/3}, \qquad (34)$$

suggesting $\kappa_f = 2/3$.

We evaluate the surface slope profile $s(y)$ in avalanche-correlated dynamics MC runs, in terms of the difference with respect to the uncorrelated case,

$$\Delta s(y) = s(y) - s_f(y) \sim y^\kappa. \qquad (35)$$

The FSS analysis for the exponent κ (the right panel of Fig. 12) yields $\kappa = 1.05 \pm 0.07$. This is in agreement with $x_{sc} = z$ and $\kappa = x_{sc}/z$ implied by the corrections to scaling formalism (24).

Inside the bulk of an avalanche the interface is fully refreshed, and scales as in uncorrelated KPZ dynamics. At the avalanche boundaries, the slope of the surface is biased upwards, because of the merging with previous MC runs (which are on average shifted upwards by an amount $s_c/2L_x$ each time an avalanche is triggered). This means that the Δs is proportional to the density of scars in the surface. In 1D, the scars are pointlike objects, the end points of the avalanches; but in 2D the avalanche boundaries are line objects. This nonscalar aspect makes that most line-segment contributions, when integrated along the boundaries of an avalanche, cancel out against each other.

To be more precise, $s(y)$ represents only the component of the slope in the y direction, and the magnitude of those jumps depends on the local angle θ the boundary makes with the y axis. This is an odd function, $\Delta(\theta) = -\Delta(-\theta)$, as illustrated in Fig. 13. The slope change is negative when the avalanche opens up and positive when it narrows down. The latter also implies that $\Delta(\theta)$ has opposite sign for the left and right boundary of each avalanche. Notice that, while in the lattice model θ takes only two discrete values, it renormalizes to a continuous variable at larger length scales.

Let us estimate the change in surface slope due to these scars in the same spirit as we did successfully in 1D. Consider one specific surface, and let $s_{\tilde{t}}(y)$ be the surface slope in a slice of the surface at distance y from the driving edge, averaged over all x, after $\tilde{t}$ avalanches (MC time $\tilde{t}$). The last avalanche changes this as follows. Let $w_{\tilde{t}}(y')$ be the width of this avalanche, which terminates at $y = l_{\tilde{t}}$, in slice y'. The inside area of the avalanche is completely refreshed and therefore has the same average slope $s_f(y)$ as in ordinary KPZ dynamics (totally refreshed subsequent world sheets). This leads to the following equation of motion:

$$\frac{\partial s_{\tilde{t}}(y)}{\partial \tilde{t}} = [\Delta(\theta_L) - \Delta(\theta_R)] + w_{\tilde{t}}(y)[s_f(y) - s_{\tilde{t}}(y)]. \qquad (36)$$

The first term on the right hand side represents the creation of the two new avalanche edges, and the second term represents the refreshed surface inside the new avalanche. Note that $\partial s_{\tilde{t}}(y)/\partial \tilde{t} = 0$ when this latest avalanche does not reach slice y, and that this is automatically taken care of because in that case $\theta_L = \theta_R = 0$ and $\Delta(0) = 0$, while $w_{\tilde{t}}(y) = 0$ for $y > l_{\tilde{t}}$. In the stationary state, after averaging over all possible avalanches, Eq. (36) leads to

$$\overline{w_{\tilde{t}}(y)[s_f(y) - s_{\tilde{t}}(y)]} = \overline{\Delta(\theta_L) - \Delta(\theta_R)}. \qquad (37)$$

Next, we perform an heuristic coarse-graining renormalization-type transformation. At large length scales, the average angle θ remains small, such that the right hand side can approximated as

$$\overline{\Delta(\theta_L) - \Delta(\theta_R)} \simeq a \overline{\theta_L - \theta_R} \simeq a \frac{\overline{\partial w_{\tilde{t}}(y)}}{\partial y}. \qquad (38)$$

Finally, we presume that in the stationary state it is not too bad to treat the KPZ height fluctuations deep inside the bulk of an avalanche and those near its edge as decoupled (at least in lowest order) such that

$$\Delta s(y) = \overline{s_f(y) - s_{\tilde{t}}(y)} = a \frac{\partial}{\partial y} \ln[\overline{w_{\tilde{t}}(y)}]. \qquad (39)$$

This yields $\Delta s(y) \sim y^{-1}$, exactly the power-law decay we are looking for, and consistent with all the above numerical results.

The only requirement for the latter is that $\overline{w_{\tilde{t}}(y)} \sim y^{-\xi}$ decays as a power law. Again, like in Eq. (32) for 1D, the value the critical exponent ξ does not matter. $\overline{w_{\tilde{t}}(y)}$ is equal to the average avalanche width in slice y averaged over all avalanches. It is reasonable to expect, and we confirmed numerically, that this quantity scales with the same exponent as the average width of all avalanches longer than y, i.e., as

$$\int_y^\infty w(l) P(l) dl \sim y^{1/z - \tau_l + 1}, \qquad (40)$$

which yields $\xi \simeq 1/3$.

We are now ready to represent the crossover scaling operator $O_{sc}(x)$ in terms of the scars on the surface. Consider time slice y, $O_{sc}(x) = 0$ when no scar line runs through site x, and otherwise is proportional to the angle the scar line makes with respect to the y axis. However, the sign also flips depending on whether this represents a left or right boundary of the original avalanche. The latter can be denoted by an arrow along the avalanche scar line. Alternatively, we can associate an age field $g(x,y)$ to the entire surface, representing the age of the surface segments (how many MC time steps ago site x was updated),

$$O_{sc} \sim \frac{\hat{e}_y \cdot \boldsymbol{\nabla} g}{|\boldsymbol{\nabla} g|} \tag{41}$$

with $\hat{e}_y$ a unit vector in the y direction. The denominator arises because the magnitude of the age jump across the scar line $|\boldsymbol{\nabla} g|$ does not play a role.

X. SUMMARY

In this paper, we studied a directed avalanche model inspired by the unloading of a sandbox by means of a slowly lowering wall, and the wish to setup an avalanche dynamic rule belonging to the same universality class as KPZ-type interface growth. The 2D sand surface represents the world sheet of the $1+1$D growing interface.

The scaling exponents of the avalanche distributions are directly related to the dynamical and stationary state roughness exponents z and α of KPZ growth in $1+1$D [Eq. (11)]. However, we encounter one crucial difference. From the avalanche perspective, the conventional uncorrelated MC runs correspond to completely refreshing the surface, i.e., an ensemble average over all possible initial conditions, without ever running an avalanche. From the KPZ perspective, the avalanche dynamics represents an unusual MC ensemble averaging procedure where subsequent interface world sheets only differ inside the single avalanche. This avalanche-correlated-type averaging enhances the interface roughness at time scales $y < L_x^z$, due to the scars of previous avalanches. It required a careful study, combining numerical and analytical tools, presented in the second half of this paper, to establish that these scars give rise only to larger than usual corrections to scaling and not to fundamentally different values of the global roughness scaling exponents z and α.

The effect of the scars can be represented by introducing an additional age field $g(x,y)$ to the height variables $h(x,y)$, that keeps track of how many MC runs ago site (x,y) participated in an avalanche. This age-field couples into the KPZ equation (5) as an additional term of the form uO_{sc}. The operator O_{sc} is proportional to the angle a scar makes with respect to the time axis, and can be expressed in terms of the age field as shown in Eq. (41). We establish that the coupling of this age field to the KPZ equation is irrelevant in the sense of renormalization theory, both numerically and by writing down approximate equations of motion for uO_{sc}. The scaling field u renormalizes with exponent $y_{sc} = -\alpha$ and O_{sc} scales with critical dimension $x_{sc} = -z$.

We believe that the results of our work presented here can be generalized to most "Markovian" avalanche dynamic systems with local row-by-row-type toppling rules, and that this is a promising route to improve our understanding of the scaling properties of avalanche dynamics in general.

[1] J.M. Carlson and J.S. Langer, Phys. Rev. Lett. **62**, 2632 (1989).
[2] K.E. Bassler and M. Paczuski, Phys. Rev. Lett. **81**, 3761 (1998).
[3] P. Bak, C. Tang, and K. Wiesenfeld, Phys. Rev. Lett. **59**, 381 (1987).
[4] A. Ben-Hur and O. Biham, Phys. Rev. E **53**, R1 317 (1996).
[5] D. Dhar and R. Ramaswamy, Phys. Rev. Lett. **63**, 1659 (1989).
[6] B. Tadić and D. Dhar, Phys. Rev. Lett. **79**, 1519 (1997).
[7] W. Kinzel, Ann. Isr. Phys. Soc. **5**, 425 (1983).
[8] R. Pastor-Satorras and A. Vespignani, Phys. Rev. E **62**, 6195 (2000).
[9] M. Paczuski and K.E. Bassler, Phys. Rev. E **62**, 5347 (2000).
[10] M. Kloster, S. Maslov, and C. Tang, Phys. Rev. E **63**, 026111 (2001).
[11] S.F. Edwards and D.R. Wilkinson, Proc. R. Soc. London, Ser. A **381**, 17 (1982).
[12] M. Kardar, G. Parisi, and Y.-C. Zhang, Phys. Rev. Lett. **56**, 889 (1986).
[13] C.-C. Chen and M. den Nijs, Phys. Rev E **65**, 031309 (2002).
[14] C.-S. Chin and M. den Nijs, Phys. Rev. E **59**, 2633 (1999).
[15] H. Hinrichsen, V. Rittenberg, and H. Simon, J. Stat. Phys. **86**, 1203 (1997).
[16] M. Paczuski and S. Boettcher, Phys. Rev. Lett. **77**, 111 (1996).
[17] C.-S. Chin, C.-C. Chen, and M. den Nijs (private communication).